Meteorology and Atmospheric Physics
https://doi.org/10.1007/s00703-018-0618-1

ORIGINAL PAPER

Overview of surface to near-surface atmospheric profiles over selected domain during the QWeCI project

J. N. A. Aryee[1] · L. K. Amekudzi[1] · W. A. Atiah[1] · M. A. Osei[1] · E. Agyapong[1]

Received: 20 September 2017 / Accepted: 25 June 2018
© Springer-Verlag GmbH Austria, part of Springer Nature 2018

Abstract

Assessing the evolution of surface to near-surface atmospheric fluxes is key to improving our understanding of their interactions, while further advancing climate applications. In this paper, an overview of the diurnal to seasonal evolution of some surface to near-surface atmospheric fluxes, coupled with their interactions, have been provided. Fluxes of downwelling and upwelling radiation ($SW_{\downarrow}$, $SW_{\uparrow}$, $LW_{\downarrow}$, $LW_{\uparrow}$), soil heat flux (ΔH), relative humidity (RH), rainfall (RR) and surface air temperature (T), measured from two different locations (Owabi and KNUST) and at a temporal resolution of 10 min, encompassing the quantifying weather and climate impact (QWeCI) Project period (2011–2013), were used to assess their relationship on diurnal to seasonal scales. First, diurnal assessments of the various profiles were performed. These provided information on the relatively active daytime, with the earth surface exposed to substantial $SW_{\downarrow}$, initiating rising and sinking thermals which subsequently increased T and ΔH, with reductions in RH until few hours after midday, beyond which a reversal was observed. Also, ΔH from the vegetative terrain (Owabi) was found to be directed into the surface at daytime, and released from the sub-surface layer back into the atmosphere at night time, compensating the energy loss by $LW_{\uparrow}$ from the surface. Furthermore, rainfall (RR) in both locations were found to be generally convective and occurring mostly between 1500 GMT and 2300 GMT. The relationship between net radiation (R_N) and RR is presently statistically unclear, although rainfall peaks were found to be occurring at low R_N and relatively warmer T, accompanied by high RH. Thereafter, seasonal assessments were performed to capture the monthly-averaged diurnal variabilities in the measured surface to near-surface parameters. These showed heightened daytime T, ΔH and R_N, coupled with relatively low RH within the dry seasons, and more reduced profiles within the monsoon season. Additionally, countrywide assessments were performed using ERA-5 datasets which showed similarities with the in situ data. However, convective rains over the domain were not fully resolved in ERA-5. Nonetheless, the findings of this study are essential to understanding surface energy balance processes in tropical, humid climates, which is important for various climate-impact modeling applications and policy formulations over the region.

1 Introduction

In a developing country, such as Ghana, where most of its economy-thriving activities are weather and climate-dependent, there is the need for scientific research to understand the dynamics of these surface to near-surface atmospheric fluxes. Information regarding diurnal to seasonal evolution of surface to near-surface atmospheric fluxes, although currently limited, remain vital to climate-impact modelling applications, as well as, improving productivity in climate-dependent sectors—which include agriculture, power generation, water resource management, geospatial planning, among others—with a compounding economic improvement.

A number of early studies have been performed regarding interactions of surface to near-surface atmospheric fluxes, and their diurnal to seasonal evolution (Steiner et al. 2009; Jhajharia and Singh 2011; Jhajharia et al. 2012; Kalthoff et al. 2018). First, it is important to note that the Sun is the driver of almost all processes on Earth, as such, variability in its output—by way of rotation of the Earth, as well as, solar declination—initiates a corresponding variation in other atmospheric variables. Previous studies channelled towards understanding some of these interactions include

Responsible Editor: A.-P. Dimri.

✉ J. N. A. Aryee
jeff.jay8845@gmail.com; jeff.jay88@yahoo.com

[1] Meteorology and Climate Science Unit, Department of Physics, Kwame Nkrumah University of Science and Technology, Kumasi, Ghana

Published online: 04 July 2018

that of Bristow and Campbell (1984), where the authors assessed the relationship between incoming solar radiation and daily maximum and minimum temperature using a simple site-specific model. The authors found the model to account for 70–90% of variation in daily solar radiation, and a complementing temperature variation. Furthermore, Dai et al. (1999) also identified over most land areas that clouds, combined with secondary damping effects from soil moisture and precipitation reduce diurnal range of surface air temperature by about 25–50% compared with clear-sky days. The authors critically assess the role of clouds in modulating the net radiation (R_N), which further modulates the diurnal range of surface air temperature. They further highlighted that approximately 80% of the variance of diurnal range of surface air temperature can be explained by cloud and precipitation variabilities.

Again, findings of Steiner et al. (2009) suggest that atmosphere-land surface coupling can impact regional-scale circulation and precipitation in regions depicting strong hydroclimatic gradients. Moreover, Jhajharia et al. (2012) studied the trends in evapotranspiration over India, and found significant decrease in the pre-monsoon season. The authors associated these decreases to the net radiation and wind speed, indicating that the decrease in wind speed and net radiation likely decreased evapotranspiration in humid regions of their study domain, in addition to their impact of temperature increases on evapotranspiration. Generally, precipitation reduces DTR mainly by decreasing surface solar radiation through increased cloud cover and by increasing daytime surface evaporative cooling through increased soil moisture content (Van den Hoof and Garreaud 2014). However, Jhajharia and Singh (2011) found that the negative correlation between DTR and precipitation does not hold globally; no correlations are observed in different climate regions. In another study, Parker et al. (2017) described the surface energy balance and its interactions within the atmospheric surface layer. A comprehensive description of the diurnal interactions of various climate variables were provided, using observations from the African Multidisciplinary Monsoon Analysis (AMMA) field campaign over selected locations in West Africa. Generally, these studies establish the baseline of surface to near-surface atmospheric flux interactions, however, the order of interaction is still spatially limited.

Such assessments—especially, diurnal to seasonal evolution of surface to near-surface atmospheric flux from ground observations—are locally limited partly because of the sparse distribution of weather stations countrywide and their irregular observation times. In Ghana, just as several other developing countries, most weather records are manually retrieved by field observers, and at particular synoptic times, thus, limiting the potential for a dense collection of field observations to support diurnal assessments of these surface to near-surface atmospheric fluxes. In 2010, the QWeCI (quantifying weather and climate impacts) project installed an automated weather station (AWS) in Owabi to provide high temporal resolution surface to near-surface atmosphere records that will form precursors for quality climate-impact assessments on vector-borne diseases over the study domain. Also, the Kwame Nkrumah University of Science and Technology (KNUST) Energy Center installed an AWS within its facility to assess the potential of harnessing solar radiation availability for solar energy and applications.

Data retrieved from these locations are used in this study for a dual purpose: (1) to provide an overview of the diurnal to seasonal evolution of surface to near-surface atmospheric fluxes and (2) to provide a highlight on the interactions of these atmospheric fluxes. This study will serve as relevant background information to the DACCIWA (Dynamics-Aerosol-Chemistry-Cloud Interactions in West Africa) project, considering Kumasi is one of the DACCIWA supersites, and assessments of planetary boundary layer (PBL) evolution and dynamics relate to the evolution and dynamics of surface to near-surface atmospheric fluxes (Knippertz et al. 2015; Flamant et al. 2017). In this study, surface to near-surface atmospheric variables, comprising surface air temperature, precipitation, soil heat flux, relative humidity, downwelling and upwelling shortwave and longwave radiations, from two automated weather stations have been assessed towards understanding their diurnal-to-seasonal evolution, as well as, their interaction. Next, these variables were used as proxies to validate ERA-5 surface flux data over the selected locations. Thereafter, the ERA-5 data was used to provide countrywide assessments of surface to near-surface atmospheric variables.

The remaining part of the study is catalogued as follows: Description of the study area and data source have been presented in Sect. 2, with the results and discussions provided in Sect. 3. Finally, conclusions are given in Sect. 4.

2 Description of study area and data source

2.1 Study area and ancillary data

Ancillary data, comprising of upwelling and downwelling shortwave and longwave radiations ($SW_{\downarrow}$, $SW_{\uparrow}$, $LW_{\downarrow}$, $LW_{\uparrow}$), surface air temperature (T), relative humidity (RH), soil heat flux (ΔH) and rainfall amount (RR), were sampled at 10 min temporal resolution for a three-year period (2011–2013) from Owabi and Kwame Nkrumah University of Science and Technology (KNUST) Energy Center (see Fig. 1). Both locations are in the forest zone of Ghana, where climatic conditions are highly variable on diurnal to seasonal scales, due to its vast vegetation cover and variable elevations. Weather conditions are mostly humid (> 50%), with average surface

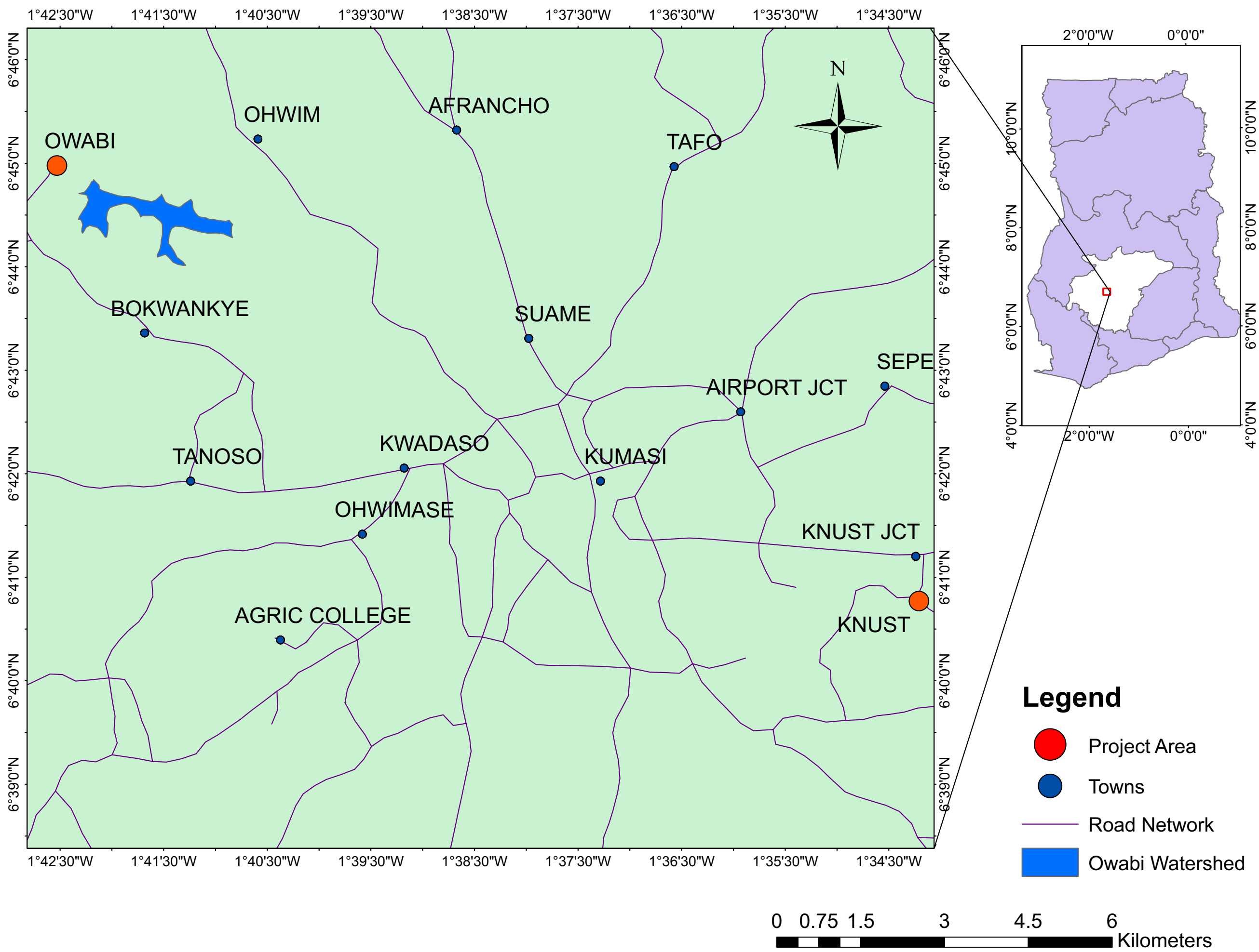

Fig. 1 Map of the Ashanti Region (left), projected from Ghana (in small upper panel), and indicating the location of the study area

temperatures ranging between 28 and 34 °C. Rainfall within this zone is monsoonal and bimodal (Aryee et al. 2018), with onsets by third dekad of March and cessation by the first dekad of November (Amekudzi et al. 2015; Mensah et al. 2016; Baidu et al. 2017).

Automated weather systems (AWS) were installed on both locations to monitor atmospheric variabilities and provide detailed observations. The radiometers were used to measure the upwelling and downwelling radiation fluxes, while the rain gauge provided information on the rainfall amount. The air temperature data was measured using the ventilation resistant thermometers placed 2 m above the ground, as described in Quansah et al. (2014). On the vegetative terrain, the soil heat flux sensor was buried about 6 cm from the surface. Details of observations made from each site is shown in Table 1.

To analyse the relative response times of the various surface to near-surface fluxes in response to changes in R_N, Pearson's correlation was employed, as discussed in Amekudzi et al. (2016) and Aryee et al. (2018), at varying lag times.

2.2 ECMWF re-analysis 5 (ERA-5) climate data

For countrywide analysis, European Centre for Medium-Range Weather Forecasts (ECMWF) Re-analysis 5 (hereafter termed as ERA-5) was first validated with data from the two locations, serving as proxies to evaluate the performance of ERA-5. ERA-5 is a climate re-analysis dataset, covering the period 1950 to present, processed by The European Center for Medium-Range Weather Forecasts (ECMWF). A major limitation of ERA-Interim that led to the generation of ERA-5 is the inaccurate representation of tropical surface net solar radiation and total precipitation. These issues have been addressed in the development of ERA-5, thus the need for such validation before making use of the dataset. Major advantages of ERA-5 are its high spatial (approximately 31 km globally) and temporal (every 1 h) resolution, which

Table 1 Description of the study locations, and the observed surface to near-surface atmospheric fluxes from each location

Location	Longitude	Latitude	Elevation [MSL]	Terrain	Observed parameters
Owabi	1° 42′ 14″ W	6° 44′ 49″ N	238 m	Vegetative, low grass near open water (dam)	$SW_{\downarrow}$, $SW_{\uparrow}$,$LW_{\downarrow}$, $LW_{\uparrow}$, ΔH, T, RH, RR
KNUST	1° 33′ 54″ W	6° 40′ 22″ N	300 m	Flat, cemented roof-top with tall buildings in vicinity	SW_N,LW_N, T, RH, RR

Four radiation components were measured at Owabi, whereas for KNUST, net shortwave and longwave were retrieved. Heat flux was only measured from the vegetative terrain (Owabi)

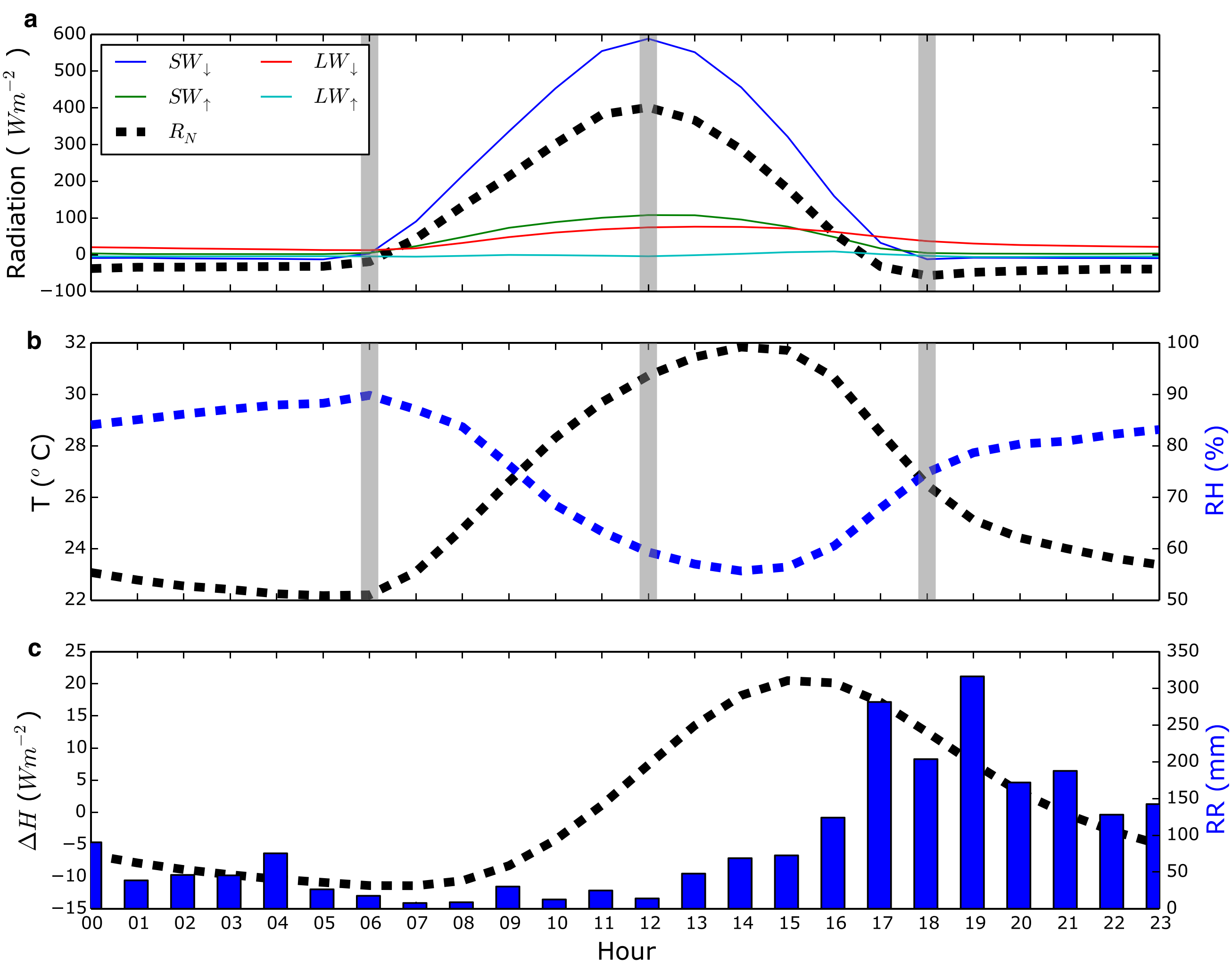

Fig. 2 Diurnal distribution of surface to near-surface parameters: **a** radiation profiles (consisting of $SW_{\downarrow}$, $SW_{\uparrow}$, $LW_{\downarrow}$, $LW_{\uparrow}$ and R_N), **b** surface air temperature and relative humidity, and **c** rainfall (in bars) and soil heat flux measured at Owabi. Grey shadings indicate sunrise, midday and sunset hours

perfectly meet the needs for quality diurnal surface to near-surface atmospheric flux assessments.

3 Results and discussion

Figure 2 shows the diurnal evolution of radiation fluxes ($SW_{\downarrow}$, $SW_{\uparrow}$, $LW_{\downarrow}$, $LW_{\uparrow}$, R_N), surface air temperature, relative humidity and soil heat flux profiles, as well as, the diurnal distribution of rainfall at Owabi. First, as clearly depicted in Fig. 2a, solar activity was heightened from sunrise to midday, beyond which there was a decline. Downwelling shortwave radiation ($SW_{\downarrow}$) was high between the sunrise and sunset hours due to the presence of the sun, and greatly influenced the net radiation flux. Moreover, it was observed from Fig. 2a that the longwave profiles lagged that of the shortwaves by approximately an hour. This implied that the re-emission of longwave radiation by the earth surface into the atmosphere was not instantaneous, in response to the downwelling shortwave radiation (Moore, 1976). Consequently, a lagged-response was observed in the diurnal profiles of both T and RH, as shown in Fig. 2b and Table 2. These profiles were analogous to $LW_{\downarrow}$, and highlighted the importance of $LW_{\downarrow}$ to modulating both the surface temperature and relative humidity profiles. Profiles of RH and T were inversely related, as such, night times were found to be extremely moist whereas surface moisture was reduced during the day. Moreover, peak temperatures were found to occur mostly between 1400 GMT and 1500 GMT, corresponding to the hours of lowest humidity.

Similarly, the diurnal evolution of R_N, T and RH from KNUST was assessed (see Fig. 3). Radiation flux patterns were again found to be similar to that of Owabi, with the net shortwave radiation (SW_N) primarily determining the magnitude of R_N, and with peaks recorded during the daytime. In response to the diurnal evolution of R_N, the surface air temperature (T) was observed to be directly related whereas RH showed an inverse relation, with both lagging R_N on order of 2–3 h. Patterns analysed in Fig. 3b suggest a marginal delay in the response of T and RH from KNUST, as compared to Owabi: which is likely attributable to the high albedo of KNUST. This contributes to higher reflectivity from KNUST, thereby reducing the temperature and humidity response to a change in R_N. On the other hand, RR over this domain was observed to be convective and mostly occurring in the evening (between 1500 GMT–2300 GMT), beyond peak R_N hours, similar to findings of Kalthoff et al. (2018).

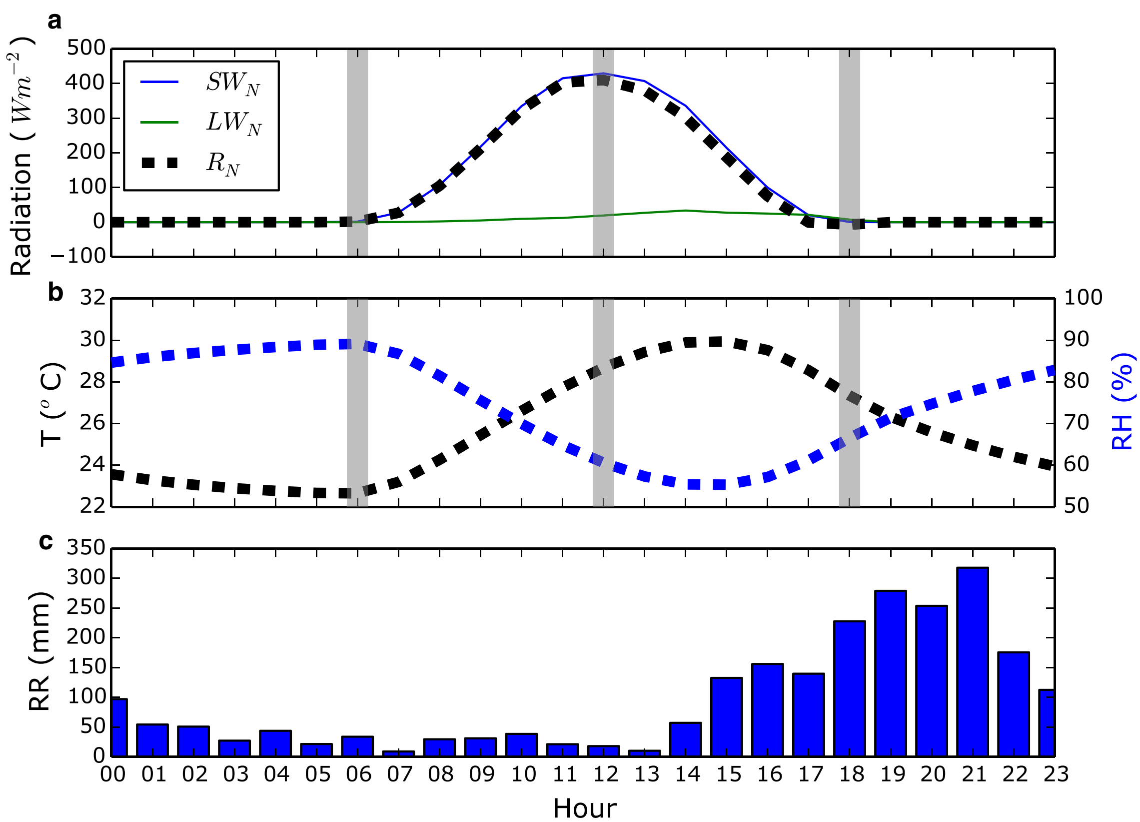

Fig. 3 Diurnal distribution of surface to near-surface parameters: **a** radiation profiles (consisting of SW_N, LW_N and R_N) and **b** surface air temperature and relative humidity measured at KNUST. Grey shadings indicate sunrise, midday and sunset hours

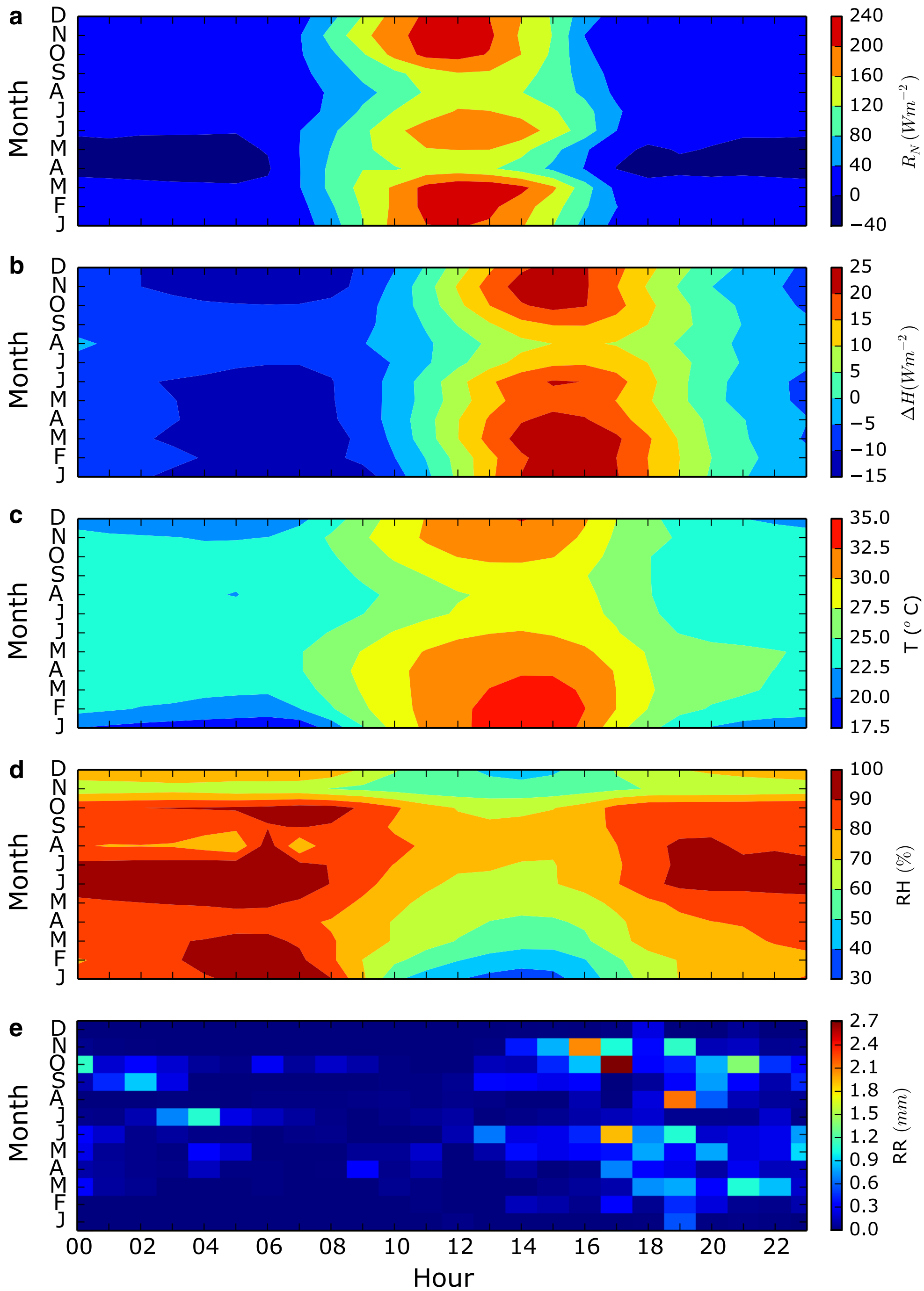

Fig. 4 Diurnal–seasonal distribution of **a** net radiation, **b** heat flux, **c** surface air temperature, **d** relative humidity and **e** rainfall measurements made from Owabi

The seasonal assessments further highlighted the monthly-mean diurnal evolution of the various surface to near-surface atmospheric fluxes over Owabi. Generally, R_N was observed to be large between 0600 UTC and 1800 UTC, depicting hours of solar activity (see Fig. 4a). At nighttime, R_N was approximately 0. Moreover, daytime R_N of dry months (November–March) were observed to be relatively higher than the rainy periods. Possible explanation is the dry state of the atmosphere within the dry seasons, with less moisture content which implies lesser reflection of $SW_{\downarrow}$ radiation. In addition, it was observed that few hours after sunset, the surface energy balance was maintained by the soil heat flux by way of radiational cooling. As shown in Fig. 4b, ΔH lagged R_N by approximately 3 h. This implied that after sunset ($R_N \rightarrow 0$), ΔH maintained the energy balance on the earth surface.

Furthermore, the temperature profiles were found to be analogous to R_N, with about 2 h lag (see Fig. 6 and Table 2), indicating on average, the time interval for a change in radiation to reflect in a corresponding T change. These T changes, in response to R_N, also showed an inverse relation with RH. To buttress the results in Fig. 2c, RR over the study domain were found to be convective almost all year, occurring mostly between the hours of 1500 GMT and 2300 GMT. However, as shown in Fig. 6 and Table 2, there was no direct linear relationship between R_N and RR. Nonetheless, Fig. 4 highlighted the contribution of R_N to the temporal distribution of RR over the study domain.

The seasonal patterns in KNUST were found similar to that of Owabi. In response to the diurnal evolution of R_N, it was observed that T and RH lagged on order of 2–3 h, representing marginal delay in the response of T and RH

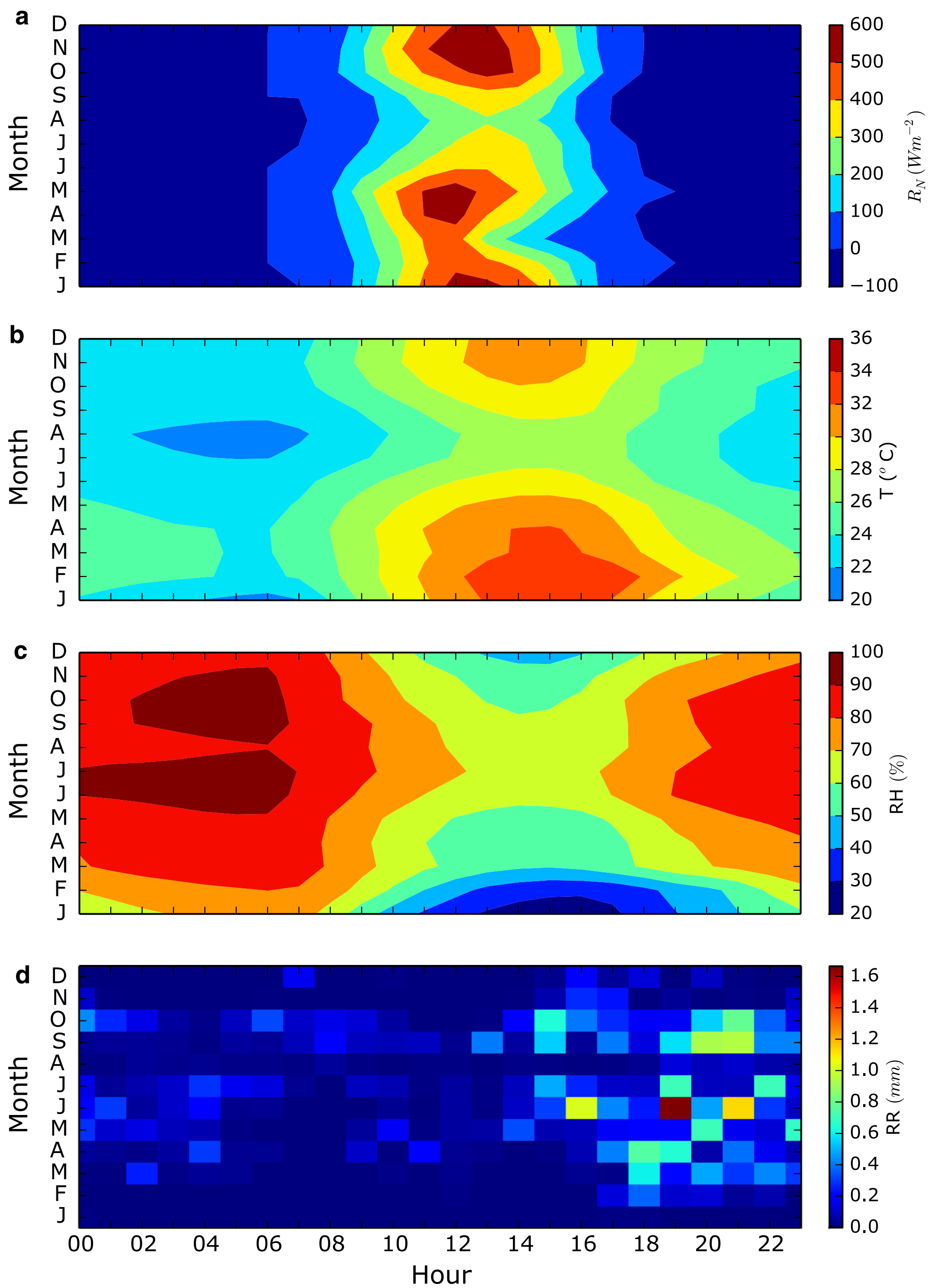

Fig. 5 Diurnal–seasonal distribution of **a** net radiation, **b** surface air temperature, **c** relative humidity and **d** rainfall measurements made at KNUST

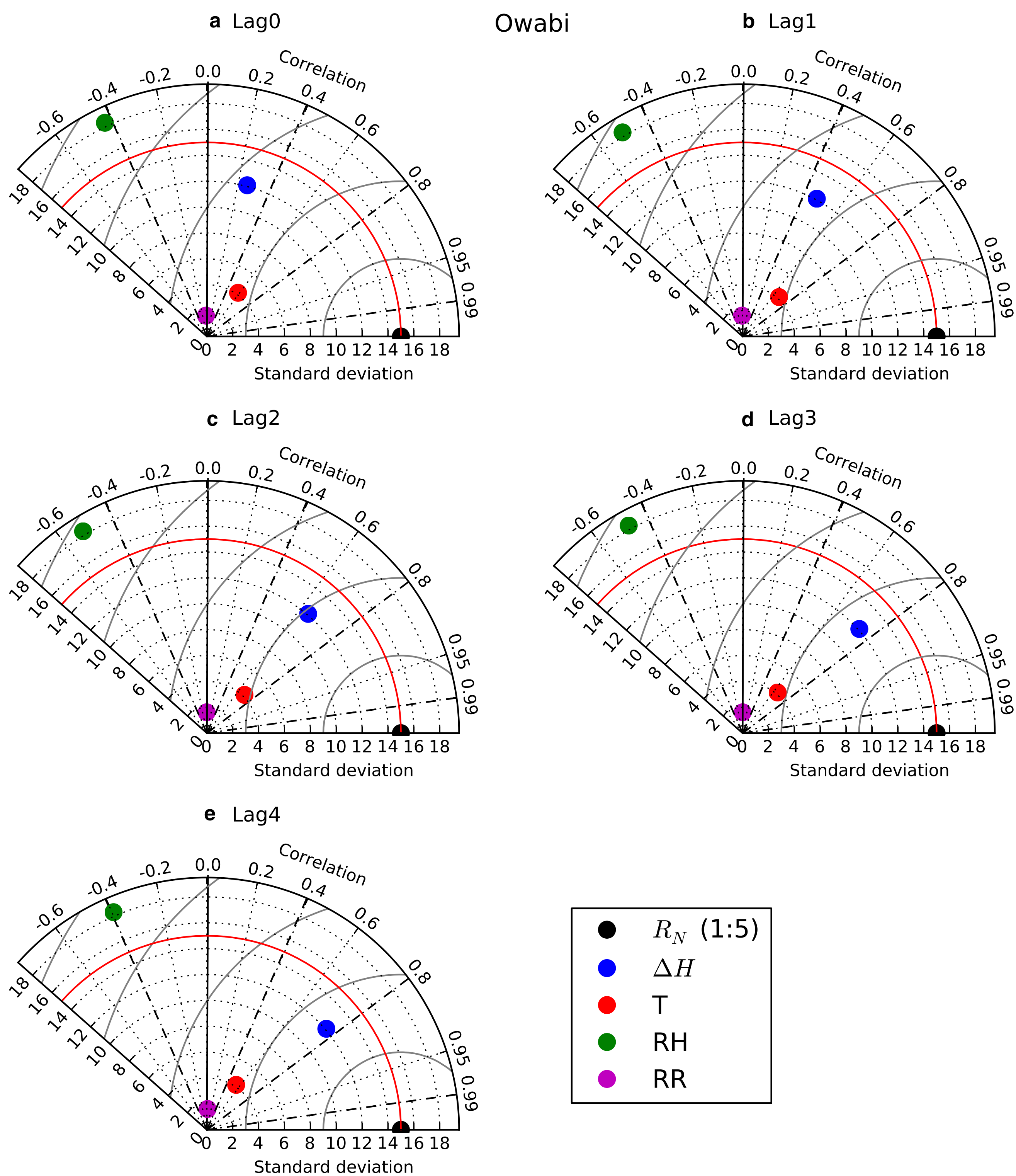

Fig. 6 Taylor diagram showing relationship of R_N with other variables at **a** Lag 0, **b** Lag 1, **c** Lag 2, **d** Lag 3 and **e** Lag 4, from the vegetative terrain

to R_N (see Fig. 5). Also, no statistical coherency was found between R_N and RR, however, rainfall events were found to be sporadic and mostly occurring beyond the peaks of R_N, precisely between 1500 GMT and 2300 GMT.

3.1 Statistical assessment of observed surface to near-surface atmospheric fluxes

The relative response in T, RH, RR and ΔH, yielding from a diurnal change in R_N has been assessed with Pearson's

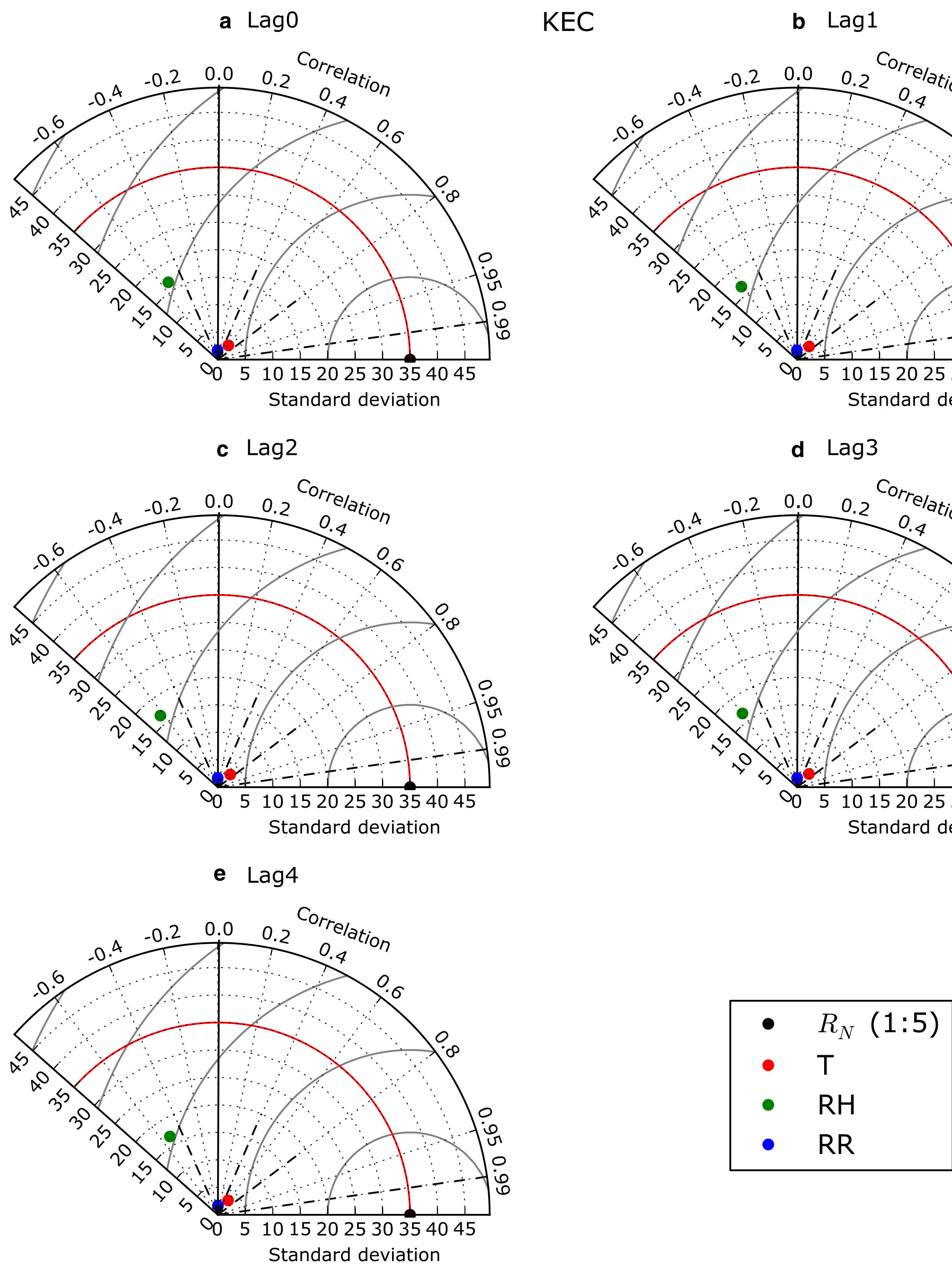

Fig. 7 Taylor diagram showing relationship of R_N with other variables at **a** Lag 0, **b** Lag 1, **c** Lag 2, **d** Lag 3 and **e** Lag 4, from the flat terrain

Table 2 Summary of correlation at different lagged times, showing the interaction of R_N with ΔH, T, RH and RR

	Site	$R_N - \Delta H$	$R_N - T$	$R_N - RH$	$R_N - RR$
Lag 0	Owabi	0.257	0.581	− 0.431	− 0.046
	KNUST	–	0.595	− 0.539	− 0.036
Lag 1	Owabi	0.474	0.679	− 0.507	− 0.029
	KNUST	–	0.675	− 0.608	− 0.029
Lag 2	Owabi	0.647	0.700	− 0.523	− 0.013
	KNUST	–	0.699	− 0.626	− 0.019
Lag 3	Owabi	0.746	0.652	− 0.481	0.003
	KNUST	–	0.664	− 0.596	− 0.003
Lag 4	Owabi	0.764	0.545	− 0.394	0.030
	KNUST	–	0.578	− 0.522	0.009

Maximum co-efficient usually indicate interval of response for each surface to near-surface variable. Variables with higher lag 0 coefficients are those with an instantaneous response to a R_N change. Lags 1, 2, 3 and 4 indicate 1, 2, 3 and 4 h interval for response, respectively, of any variable to R_N change. All correlation coefficients were found statistically significant at 99% confidence level

correlation analysis—at varying lag times—and illustrated on Taylor diagrams, with a summary of the correlation coefficients provided in Table 2. Taylor diagrams provided in Figs. 6 and 7, have correlation coefficients indicated on the outer edges of the quadrant. Each method's correlation is deduced via linking the zero-mark to the edge of the quadrant through the individual point. For Owabi, optimal response times of T and RH, with respect to change in R_N was 2 h, with T showing a direct relationship while RH showed an inverse relationship. Additionally, ΔH had highest positive correlation at lag-4, showing a response time of 4 h for a change in R_N to induce a change in soil heat flux at Owabi. At KNUST, response time of T and RH, in relation to change in R_N was 2 h, with T showing a direct relation while RH showed an inverse relation (see Fig. 7). In both locations, RR had no correlation with R_N, as illustrated in Figs. 6 and 7: indication of a strong limitation in using only R_N as determinant for RR. Nonetheless, it was observed (see Figs. 2c, 4e), that rainfall events were mostly sporadic, but with majority of them occurring at nighttime, beyond the peak hours of R_N, which confirms findings of Kalthoff et al. (2018). Summaries of the lag-0 to lag-4 comparisons have been provided in Table 2, with all coefficients found statistically significant at 99% confidence level.

3.2 Validation of ERA-5 hourly forecast data

Reproducing similar assessments over the entire country is essential to understanding countrywide interactions of these surface to near-surface atmospheric fluxes. Nonetheless, the Ghana Meteorological Agency (GMet) does not perform hourly observation of these variables over the entire country, and these serve as limitation for such diurnal assessments. Hence, ERA-5 forecast climate data, which has a higher spatio-temporal resolution, has been validated via daily accumulations and averages using GMet standard records [not shown], and thereafter used for countrywide diurnal assessment of the surface to near-surface atmospheric fluxes.

3.3 Overview of countrywide variations in surface to near-surface atmospheric fluxes

In this section, the surface to near-surface atmospheric fluxes were averaged for every 6 h and also on seasonal basis, to capture their diurnal patterns and evolution, as well as, their seasonal variabilities. In Fig. 8, the entire country was characterized by extremely low R_N values all year, which ranged between −80 and 0 W m^{-2}. Temperature values also ranged from 294 to 304 K. Within the pre-monsoon season (MAM), the northern portion of the country was characterized by relatively higher pre-sunrise temperatures. Moreover, within these hours, the entire country's surface is moist except the northern parts in the dry (DJF) and pre-monsoon (MAM) seasons where RH ranged between 60 and 80%. On average, RR was typically less than 3 mm/h and ΔH was less than 10 W m^{-2} for pre-sunrise hours over the country. The DJF season recorded negative ΔH values in the northern half of the country.

In addition, Fig. 9 captured the sunrise to noon profiles of surface to near-surface atmospheric fluxes over the country. R_N values were observed to range from approximately 50 W m^{-2} in the West to 320 W m^{-2} in the north-eastern borders. Also, average temperatures ranged between 294 K and 308 K, with patterns similar to R_N. Again, the pre-monsoon season recorded relatively higher temperatures in the northern half of the country and the region of the Volta Lake, as shown in Fig. 9. Consequently, countrywide RH were relatively less than the earlier hours, ranging from 60 to 100%. The northern half was less moist than the southern parts, especially within the dry (DJF) season. Furthermore, seasonal rainfall patterns from ERA-5 captured more rains in the monsoon season (JJA), especially in the west Coast of the country and the eastern borders, which confirms the findings of Amekudzi et al. (2015) and Aryee et al. (2018). Also, the pre-monsoon and the minor rainy season (SON) recorded some amount of rains. Rainfall over the country were on order of up to 4 mm/h. Moreover, ΔH values observed within the study period ranged, on average, from 10 to 30 W m^{-2}.

The 1200–1700 GMT period was characterized by peaks in the surface to near-surface atmospheric fluxes, as shown in Fig. 10. R_N ranged from 240 to 560 W m^{-2}, with relatively reduced R_N profiles in the monsoon season (JJA), likely attributable to reduced $SW_{\downarrow}$ due to the presence of stratiform clouds. Also, surface temperature profiles were observed to

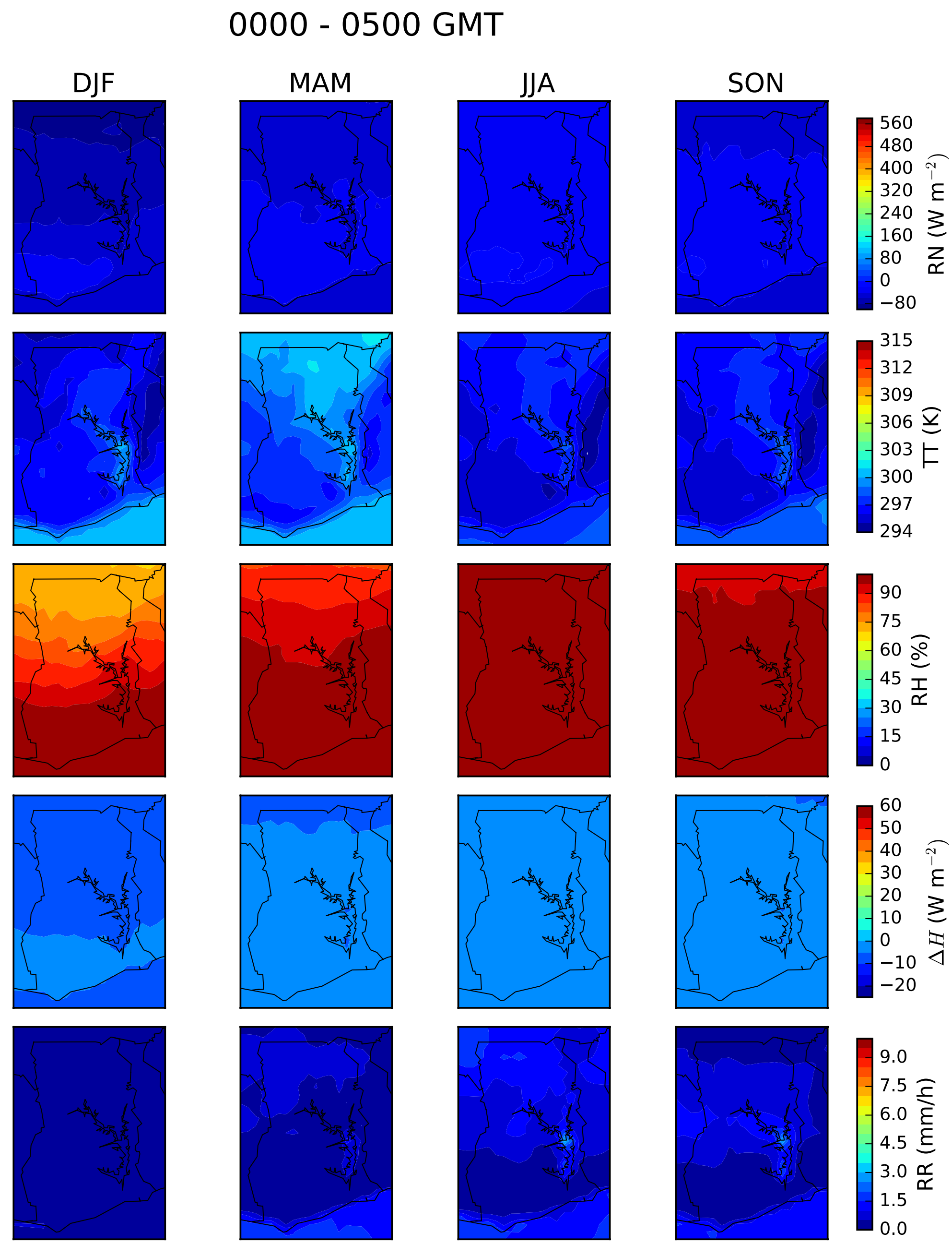

Fig. 8 Countrywide profile of R_N, TT, RR, ΔG for 0000–0500 GMT, retrieved from ERA-5

range between 298 and 314 K. Again the northern half of the country depicted relatively warmer pre-monsoon temperatures. Relative humidity further decreased, with values ranging from 60–80%. Also, rainfall seasonal patterns were similarly captured as that of the 0500–1100 GMT profile, however, rainfall rate was quite higher in comparison to the earlier profiles, with the coast and eastern borders recording values on the order of 5–9 mm/h. Additionally, ΔH was observed to range between 25–55 W m^{-2} with relatively high fluxes captured over the mid-portion of the country in DJF and the northern half of the country in the remaining seasons, especially MAM.

In Fig. 11, there is a decline in the countrywide surface to near-surface atmospheric fluxes. For example, net radiation flux reduced to approximately −80 to 90 W m^{-2}, with the coastal portions relatively higher than the northern parts, especially in the DJF and SON seasons. Also, temperatures were observed to range between 297 and 307 K. Similarly, the northern part of the country and the domain of the Volta River recorded relatively higher temperatures, especially within the pre-monsoon

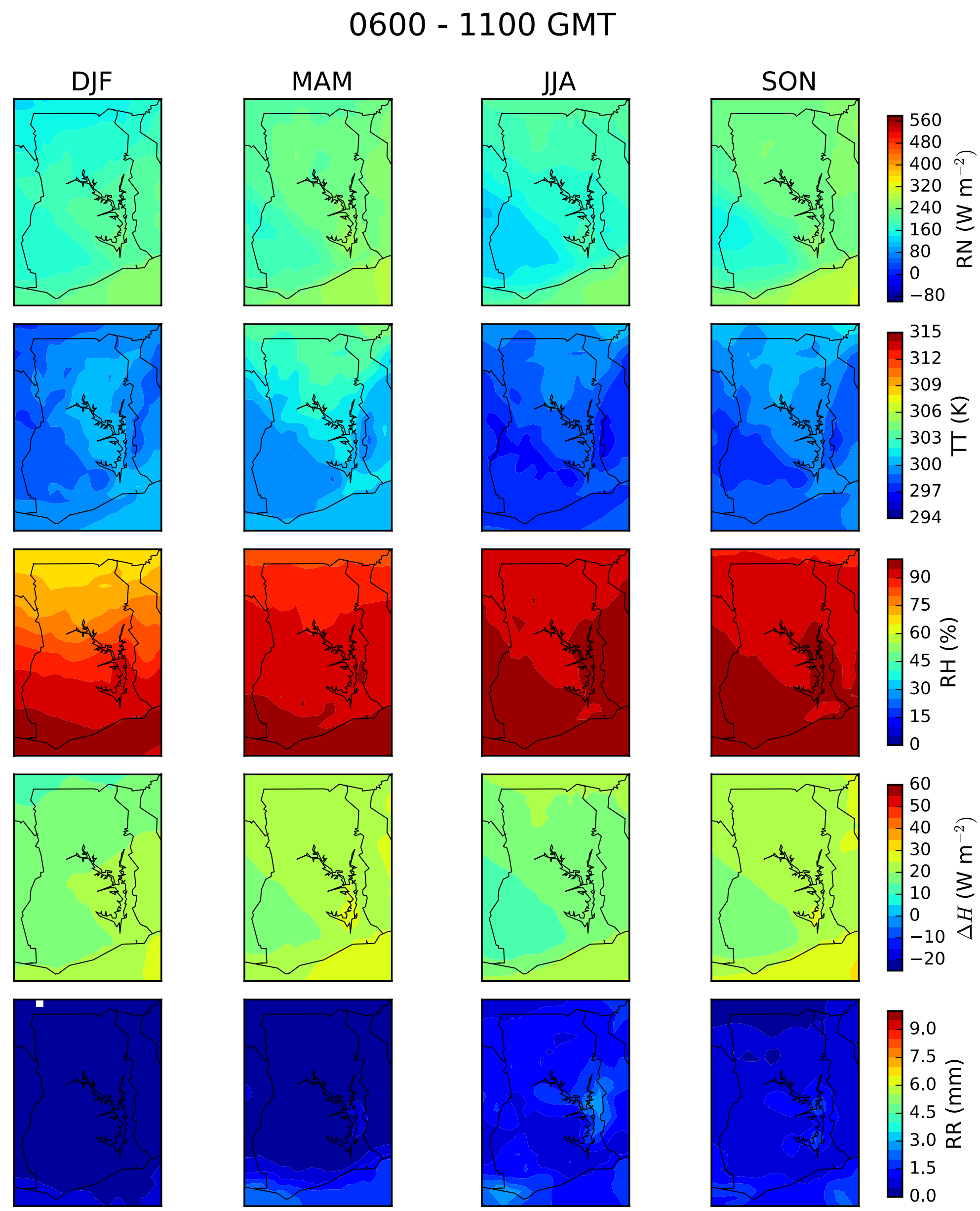

Fig. 9 Countrywide profile of R_N, TT, RR, ΔH for 0600–1100 GMT, retrieved from ERA-5

season (MAM). On average, RH increased from the 1200–1700 GMT profile, with values of 60–100%. Contrary to earlier point-based in situ observations and literature above-discussed, ERA-5 observed the coastal part of the country to be relatively dry between the hours of 1800–2300 GMT, with rain rates below 2 mm/h. RR values were up to 5 mm/h in the middle and northern part of the country. This, coupled with earlier observations, indicate an early resolving of convective rains by ERA-5 between 1200–1700 GMT, and inadequate resolution of rains between the hours of 1800–2300 GMT. This underperformance of ERA-5 confirms the findings of Massari et al. (2017). Furthermore, ΔH was observed to be less than 5 W m^{-2} over the entire country.

3.4 Relevance of findings

This study is relevant first for the modeling community because it provides information on the lag in response times of the surface to near-surface atmospheric fluxes with

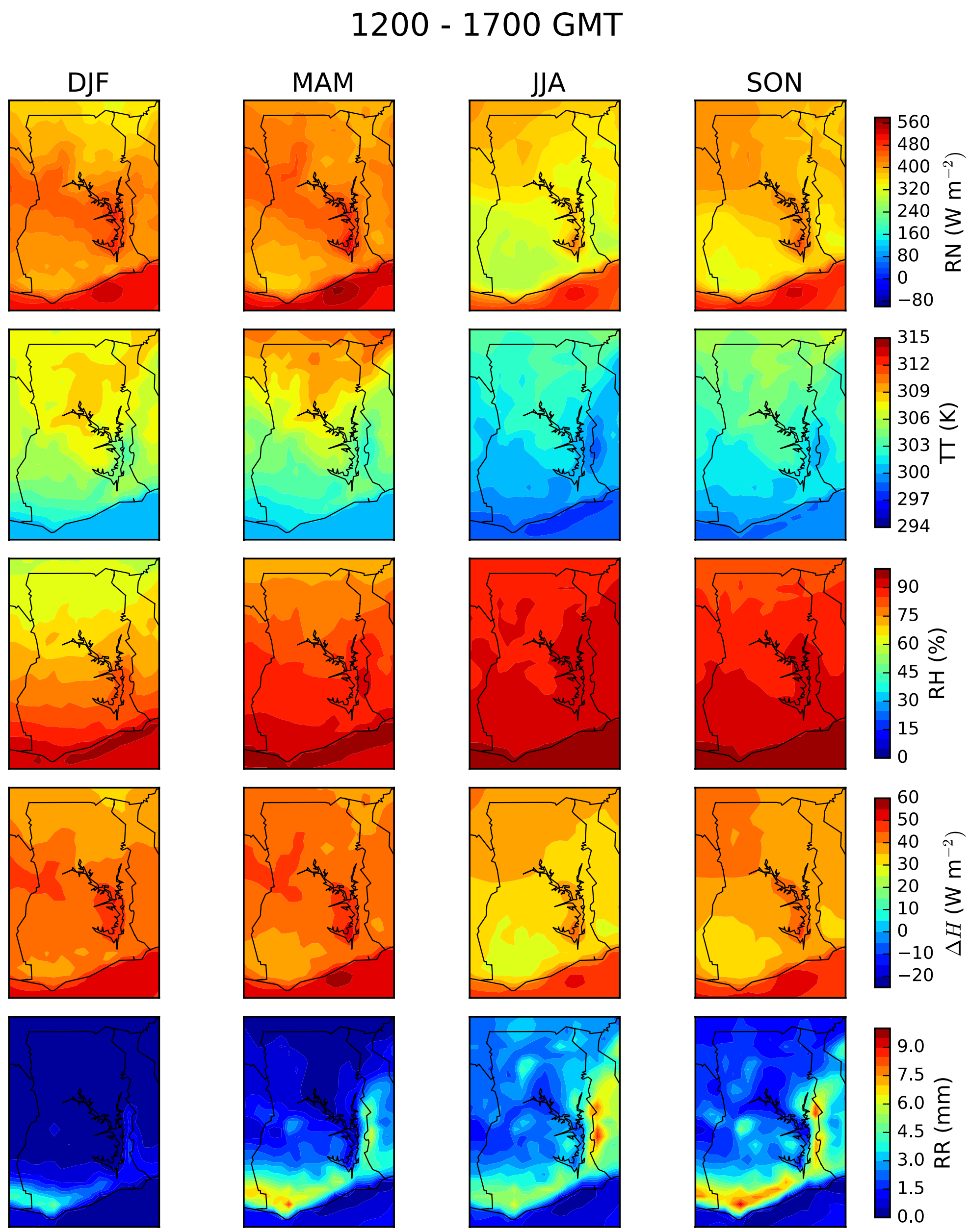

Fig. 10 Countrywide profile of R_N, TT, RR, ΔH for 1200–1700 GMT, retrieved from ERA-5

respect to changes in R_N over the country. Also, it provides information on the inability of ERA-5 to fully resolve diurnal precipitation processes in this domain (Massari et al. 2017), since it fails to capture the characteristic convective rains of this domain, occurring especially beyond peak R_N hours. Moreover, the study provides the diurnal to seasonal profiles of surface to near-surface atmospheric fluxes which is of great interest to the climate-dependent sectors such as the agricultural sector, considering the predominant farming type countrywide is rain-fed, and dependencies on the other profiles as well as its seasonal variabilities provide information on onsets, cessation and length of the growing season to this sector (Amekudzi et al. 2015; Mensah et al. 2016; Asamoah et al. 2017). The study further provides a highlight on the surface flux profiles over the country, and this sets the tone for planetary boundary layer assessments (which are currently ongoing) from the DACCIWA (Dynamics-Aerosol-Chemistry-Cloud Interactions in West Africa) field campaign data.

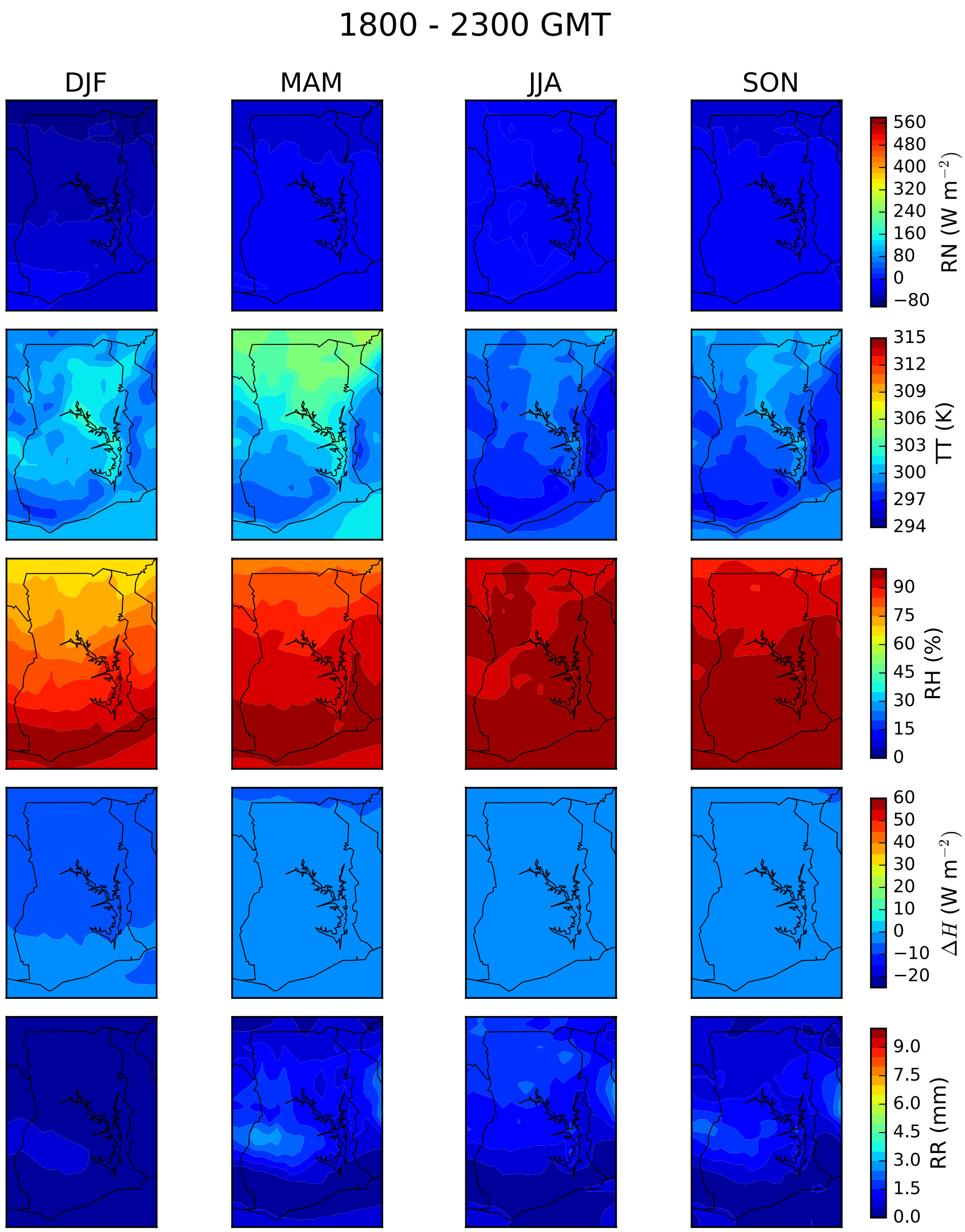

Fig. 11 Countrywide profile of R_N, TT, RR, ΔH for 1800–2300 GMT, retrieved from ERA-5

4 Conclusions

In this paper, diurnal to seasonal evolution of surface to near-surface atmospheric fluxes, and their interactions have been assessed over (i) two selected domains—Owabi and KNUST and (ii) the entire country, with data spanning the period of the QWeCI project (2011–2013).

Generally, the diurnal assessments provided information on the relatively active daytime with R_N profiles increasing from sunrise to midday, beyond which a reversal was seen. Similar trends were observed for both T and RH, however lagging R_N by 2 h, and with RH depicting an inverse evolution. Also, diurnal evolution of ΔH showed similarity with R_N and T, however lagging on order of 4 and 2 h respectively. ΔH was directed into the surface at daytime, whereas at night time, it was released from the sub-surface layer back into the atmosphere and thus compensated the energy loss by $LW_{\uparrow}$ from the surface. Additionally, no direct diurnal relationship was observed between R_N and RR. However, in Owabi and KNUST, RR was found to be mostly convective, sporadic and occurring after peak R_N, between the hours of 1500 GMT and 2300 GMT. Contrary to diurnal rainfall patterns observed by the AWS in Owabi and KNUST, the ERA-5 precipitation data resolved convective rains earlier (1200–1700 GMT) over the entire country, and underestimated the rains between 1800–2300 GMT.

Furthermore, the seasonal assessments showed heightened daytime T, ΔH and R_N fluxes, as well as, relatively low RH within the dry seasons, and the reverse within the rainy seasons. Moreover, R_N and RR were weakly correlated.

Additionally, a key finding of the study is the relatively high surface air temperature fluxes found in the northern half of the country and the domain of the Volta River, especially in the pre-monsoon (MAM) season. This forms a basis for detailed microscale variability assessment of surface to near-surface atmospheric fluxes in those locations, and identification of possible reasons for their nature.

In all, the findings of this study prove useful for various climate applications and, climate policy formulations and actions over the study domain, as well as, regions that depict similar climate and geomorphology.

Acknowledgements The authors greatly appreciate Prof. Andreas H. Fink for his donation of the AWS at Owabi to the Meteorology and Climate Science Unit (KNUST) after the QWeCI Project. Extra thanks to KNUST Energy Center for allowing the authors use their dataset for this study, as well as, The European Center for Medium-Range Weather Forecasts (ECMWF) which processes the ERA-5 datasets. The first three authors have also received funding from the European Union 7th Framework Programme (FP7/2007-2013) under grant agreement 603502 (EU project DACCIWA: Dynamics-Aerosol-Chemistry-Cloud Interactions in West Africa). Extra appreciation to the anonymous reviewers whose comments helped to shape this paper.

References

Amekudzi LK, Yamba E, Preko K, Asare EO, Aryee J, Baidu M, Codjoe NAS (2015) Variabilities in rainfall onset, cessation and length of rainy season for the various agro-ecological zones of Ghana. Climate 3:416–434

Amekudzi LK et al (2016) Validation of TRMM and FEWS satellite rainfall estimates with rain gauge measurement over Ashanti region. Ghana. Atmos Clim Sci 6(04):500

Aryee JNA, Amekudzi LK, Quansah E, Klutse NAB, Atiah WA, Yorke C (2018) Development of high spatial resolution rainfall data for Ghana. Int J Climatol 38(3):1201–1215

Asamoah PKB, Obodai J, Amekudzi LK (2017) The relationship between annual rainfall totals, rainfall onsets and cocoa yields in Ashanti Region of Ghana: a reality or farce? J Environ Earth Sci 7(8):85–88

Baidu M, Amekudzi LK, Aryee JNA, Annor T (2017) Assessment of long-term spatio-temporal rainfall variability over Ghana using wavelet analysis. Climate 5(2):30

Bristow KL, Campbell GS (1984) On the relationship between incoming solar radiation and daily maximum and minimum temperature. Agric For Meteorol 31(2):159–166

Dai A, Trenberth KE, Karl TR (1999) Effects of clouds, soil moisture, precipitation, and water vapor on diurnal temperature range. J Clim 12:2451–2473

Flamant C et al (2017) The dynamics-aerosol-chemistry-cloud interactions in West Africa field campaign: overview and research highlights. Bull Am Meteorol Soc (2018). https://doi.org/10.1175/BAMS-D-16-0256.1

Jhajharia D, Dinpashoh Y, Kahya E, Singh VP, Fakheri-Fard A (2012) Trends in reference evapotranspiration in the humid region of northeast India. Hydrol Process 26(3):421–435

Jhajharia D, Singh VP (2011) Trends in temperature, diurnal temperature range and sunshine duration in northeast india. Int J Climatol 31(9):1353–1367

Kalthoff N et al (2018) An overview of the diurnal cycle of the atmospheric boundary layer during the West African monsoon season: results from the 2016 observational campaign. Atmos Chem Phys 18(4):2913–2928

Knippertz P et al (2015) The DACCIWA project: dynamics-aerosol-chemistry-cloud interactions in West Africa. Bull Am Meteorol Soc 96(9):1451–1460

Massari C, Crow W, Brocca L (2017) Global evaluation of ERA-Interim (and ERA5) and other global rainfall estimates over land without ground-based observations by using Triple Collocation Analysis, Rome. 5th Int Conf Reanal (ICR5). https://doi.org/10.13140/rg.2.2.24970.57282

Mensah C, Amekudzi LK, Klutse NAB, Aryee JNA, Asare K (2016) Comparison of rainy season onset, cessation and duration for Ghana from RegCM4 and GMet datasets. Atmos Clim Sci 6(02):300

Moore C (1976) A comparative study of radiation balance above forest and grassland. Q J Royal Meteorol Soc 102(434):889–899

Parker DJ et al (2017) Local weather. In: Parker DJ, Diop-Kane M (eds) Meteorology of Tropical West Africa: the forecasters' handbook, 1st ed. Wiley, pp 130–172

Quansah E, Amekudzi LK, Preko K, Aryee J, Boakye OR, Boli D, Salifu MR (2014) Empirical models for estimating global solar radiation over the Ashanti region of Ghana. J Solar Energy. https://doi.org/10.1155/2014/897970

Steiner AL, Pal JS, Rauscher SA, Bell JL, Diffenbaugh NS, Boone A, Sloan LC, Giorgi F (2009) Land surface coupling in regional climate simulations of the West African monsoon. Clim Dyn 33(6):869–892

Van den Hoof C, Garreaud R (2014) Assessing the influence of precipitation on diurnal temperature range changes: implications for climate change projection. AGU Fall Meeting Abstract, San Francisco